Technology in Cancer Research and Treatment
ISSN 1533-0346
Volume 13, Number 6, December 2014

A Novel Technique for Image-Guided Local Heart Irradiation in the Rat

Sunil Sharma, Ph.D.[1]*
Eduardo G. Moros, Ph.D.[2]
Marjan Boerma, Ph.D.[3]
Vijayalakshmi Sridharan, Ph.D.[3]
Eun Young Han, Ph.D.[1]
Richard Clarkson, Ph.D.[1]
Martin Hauer-Jensen, M.D., Ph.D.[3]
Peter M. Corry, Ph.D.[1]

[1]Department of Radiation Oncology, Radiation Oncology Center, University of Arkansas for Medical Sciences, Little Rock, AR
[2]Department of Radiation Oncology, H. Lee Moffitt Cancer Center and Research Institute, Tempa, FL
[3]Department of Pharmaceutical Sciences, Division of Radiation Health, University of Arkansas for Medical Sciences, Little Rock, AR

www.tcrt.org
DOI: 10.7785/tcrt.2013.600256

In radiotherapy treatment of thoracic, breast and chest wall tumors, the heart may be included (partially or fully) in the radiation field. As a result, patients may develop radiation-induced heart disease (RIHD) several years after exposure to radiation. There are few methods available to prevent or reverse RIHD and the biological mechanisms remain poorly understood. In order to further study the effects of radiation on the heart, we developed a model of local heart irradiation in rats using an image-guided small animal conformal radiation therapy device (SACRTD) developed at our institution. First, Monte Carlo based simulations were used to design an appropriate collimator. EBT-2 films were used to measure relative dosimetry, and the absolute dose rate at the isocenter was measured using the AAPM protocol TG-61. The hearts of adult male Sprague-Dawley rats were irradiated with a total dose of 21 Gy. For this purpose, rats were anesthetized with isoflurane and placed in a custom-made vertical rat holder. Each heart was irradiated with a 3-beam technique (one AP field and 2 lateral fields), with each beam delivering 7 Gy. For each field, the heart was visualized with a digital flat panel X-ray imager and placed at the isocenter of the 1.8 cm diameter beam. In biological analysis of radiation exposure, immunohistochemistry showed γH2Ax foci and nitrotyrosine throughout the irradiated hearts but not in the lungs. Long-term follow-up of animals revealed histopathological manifestations of RIHD, including myocardial degeneration and fibrosis. The results demonstrate that the rat heart irradiation technique using the SACRTD was successful and that surrounding untargeted tissues were spared, making this approach a powerful tool for *in vivo* radiobiological studies of RIHD. Functional and structural changes in the rat heart after local irradiation are ongoing.

Key words: Radiation-induced heart disease; Animal model; Local heart irradiation; SACRTD.

Introduction

Radiation-induced heart disease (RIHD) is a long-term side effect of radiotherapy of intrathoracic, breast and chest wall tumors when the whole heart or part of the heart is situated in the radiation field (1-3). The main manifestations of RIHD present several years after radiation therapy and include accelerated atherosclerosis, pericardial and myocardial fibrosis, electrical conduction abnormalities, and injury to the cardiac valves (1, 4). With improved radiotherapy planning and delivery techniques, cardiac radiation exposure has been greatly reduced; however, recent studies indicate that patients with Hodgkin's disease, lung cancer, esophageal or proximal gastric cancer may still receive a high dose of radiation to part of the heart or a low dose to the whole heart (5-11). Similarly, adjuvant tangential radiotherapy, which is the common treatment of breast cancer in most

Abbreviations: RIHD: Radiation-Induced Heart Diseases; SACRTD: Small Animal Conformal Radiation Therapy Device; SAD: Source to Axis Distance; CBCT: Cone Beam Computed Tomography; DAPI: 4′,6-diamidino-2-phenylindole.

*Corresponding author:
Sunil Sharma, Ph.D.
E-mail: ssharma@uams.edu

parts of the world and until recently also in the western world, exposes small parts of the heart to doses >20 Gy in a large portion of left-sided breast cancer patients (3, 12). Moreover, although there are increasing uses of concomitant therapies, the extent to which these therapies enhance the effects of radiation in the heart is not yet known. Hence, RIHD is widely acknowledged as an impediment to quality of life for certain long-term cancer survivors. The pathogenesis of RIHD is largely unknown and, other than certain treatment planning techniques and respiration management during radiotherapy, there is no available pharmacological method to prevent its manifestations. Therefore, pre-clinical studies are required to unravel biological mechanisms of RIHD and to identify potential molecular targets for intervention.

Small animal models of heart irradiation have long been used in pre-clinical studies of radiation-induced cardiomyopathy (12-15). Both single doses and fractionated protocols lead to reduced ventricular ejection fraction and restrictive diastolic filling as measured *in vivo* (16) and reduced cardiac output and increased diastolic stiffness when measured *ex vivo* (16-18). Histopathological changes include myocardial degeneration (myocardial necrosis, accompanied by inflammation) and fibrosis. Because image-guided irradiators have not generally been available for small laboratory animals until recently, animals were usually irradiated either to the whole thorax or with relatively large AP-PA fields to expose the whole heart (19, 20).

We developed a small animal conformal radiation therapy device (SACRTD) at our institution that can mimic clinical conformal radiotherapy techniques in a pre-clinical setting. The system has onboard high resolution cone beam computerized tomography (CBCT) imaging capabilities and it uses a computer controlled robotic arm having six degrees of freedom to facilitate 3D-conformal radiation therapy delivery with high accuracy and precision. We used the SACRTD to develop a rat model of conformal heart irradiation (21-26). In this paper, we discuss the design, dosimetry, irradiation technique and biological evaluation of this rat model of RIHD.

Materials and Methods

The SACRTD System

The SACTRD consists of a 225 kVp X-ray source, a stage mounted on a robotic positioning arm and a digital amorphous silicon flat panel detector (FPD). The X-ray tube (GE Isovolt Titan 225) has focal spot sizes of 0.4 mm/3 mm and is mounted on a custom made "gantry" (26-28). Mounted on the tube is a special collimating assembly, consisting of a brass primary collimator with a thickness of 5 cm and a hole of 0.5 cm diameter, and an aluminum secondary collimator (15.5 cm long, 1.9 cm internal diameter). Different field sizes can be achieved by using interchangeable nozzles (Figure 1). Field sizes at isocenter (source to axis distance (SAD) of 32.5 cm) may include circular fields of 0.5 mm and 1 mm in diameter, and rectangular fields of $2 \times 2\,mm^2$ and $4 \times 4\,mm^2$. The stage is mounted on an Adept S650 robotic arm (Adept Technology, Pleasanton, CA) having six degrees of freedom, which is able to move and position the animal with a repeatability of ± 0.020 mm in the X, Y, and Z directions (29). The inset box in Figure 1 shows the setup for cone beam CT imaging. The X-ray source and flat panel detector are aligned and an object to be imaged is immobilized on the "palm" of the robotic arm. The $20.48\,cm^2$ FPD (1024×1024 pixels, Perkin Elmer, Fremont, CA) has a resolution of 200 µm and can acquire radiographic images at a frame rate of 7.5 Hz (30). The detailed technical and hardware information of the system is listed in Table I (30).

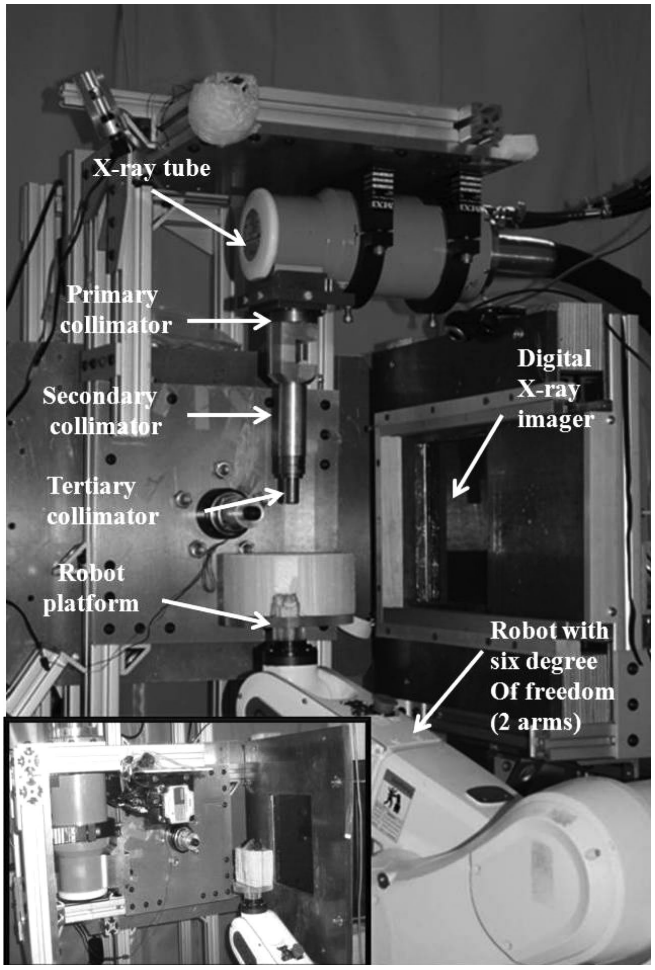

Figure 1: The small animal conformal radiation therapy device (SACRTD) at UAMS. A custom made collimator that can hold small plug-in collimators (tertiary collimators size down to 0.5 mm in diameter) is attached to the 225 kV X-ray tube, and an Adept Viper robot is used to position the target. The X-ray tube is mounted on a rotating gantry to facilitate digital X-ray imaging and therapy. The inset picture shows the setup for cone beam CT imaging.

Table I
Technical specifications of the SACRTD.

X-ray source:	GE Seifert X-ray tube Isovolt titan 225 M2
Model:	NDI 225M metal ceramic dual focal spot
Focal spot size:	0.4 mm/3 mm
Power:	640 W/3000 W
Inherent filtration	0.8 mm Be
Additional filtration:	0.5 mm Cu
Generator:	GE IsoVolt Titan 225
Target angle:	20°
Robot manufacturer:	Adept Inc., Livermore, CA, USA
Model:	Adept Viper s650
Overall arm length:	565 mm (270 mm first arm and 295 second arm)
Motion range:	J1 ± 170°, J2 = −190°, +45, J3 = −29°, +256°, J4 = ±190°, J5 = ±120°, J6 = ±360°
Maximum pay load:	5 kg
Positional repeatability:	±0.02 mm in each of X, Y and Z direction,
Drive motor and break:	AC servo motors for all joints and breaks for joint J2 and J6
Controller:	Adept smart controller and Adept T1 pendent
Flat-panel x-ray detector:	Perkin-Elmer, Wiesbaden, Germany
Model:	XRD 0820 CN3 digital x-ray detector
Detector size:	20.48 cm × 20.48 cm
Pixel matrix format:	1024 × 1024
Pixel pitch:	0.2 mm
Scintillator:	CsI (Tl)
Maximum frame rate:	7 fps

The large focal spot is used for therapy, with the system able to deliver up to 2.25 Gy/min at isocenter with the collimator designed for rat heart irradiation, as explained below. High resolution radiographic images are acquired with the small focal spot. In the image acquisition configuration, as shown in the inset box in Figure 1, the tube gantry is locked in the horizontal position, directing the X-ray beam at the FPD (typical tube voltage between 70-100 kV). The animal to be imaged is immobilized on the stage or "palm" of the robotic arm. Images can be acquired in either continuous mode or stop-and-capture mode. The detector is mounted 23 cm from the radiation/gantry isocenter and 56 cm from the X-ray source, thus producing a 1.7 image magnification factor. If necessary, other source-to-detector configurations are possible. An in-house developed software tool controls the robot motion, the X-ray activation and data acquisition by the imager. The digital planar radiographs can also be acquired over a full 360° around the specimen and used for CBCT image reconstruction, producing a full 3D image dataset. The reconstruction is done axially, slice-by-slice, using an in-house MATLAB program (Mathworks, Natick, MA, USA), which allows either a full reconstruction or only selected regions of interest to be reconstructed**.** Figure 2 shows the CBCT reconstructed sagittal, axial and coronal views of the upper section of a rat's body using a custom made vertical rat holder and the SACRTD. Three hundred and sixty planar radiographs were acquired in cone beam mode for one complete rotation of the rat (one radiograph per degree of rotation). The reconstructed image had pixel spacing of 0.18 mm × 0.18 mm × 0.18 mm in the X-Y-Z directions. The reconstructed 2D slices are stacked to create a 3D volumetric image that can be used for target localization, positioning and image guidance.

Monte Carlo Simulation and Film Dosimetry

BEAMnrc and DOSXYZnrc Monte Carlo based simulations were performed to characterize the beam collimation of the SACRTD. The simulation included the X-ray tube, a 1.0 mm Be inherent filter, a 0.5 mm thickness Cu filter, and the brass

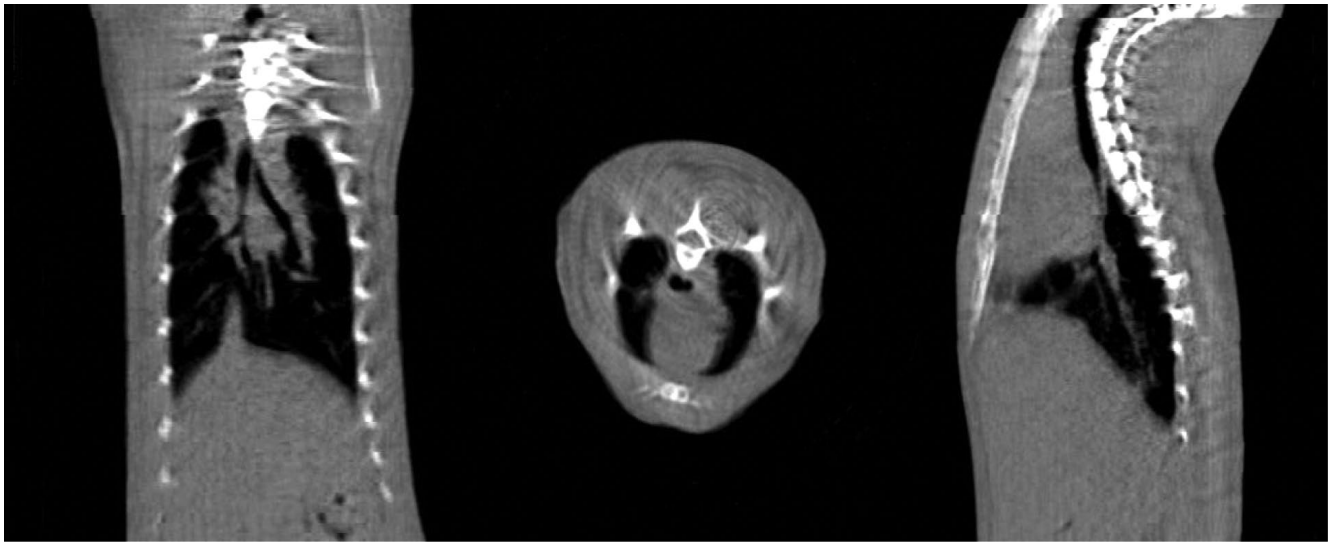

Figure 2: CBCT reconstructed sagittal, axial and coronal images of the upper section of a rat body, demonstrating the CBCT capabilities of the SACRTD. The reconstructed image has pixel spacing of 0.18 mm × 0.18 mm × 0.18 mm in the X-Y-Z directions.

primary and aluminum secondary collimators (31). A schematic diagram of the collimator design rendered by BEAMnrc in the x-z direction is shown in Figure 3. The Monte Carlo results were compared to measurements of depth dose distribution using solid water cutouts and Gafchromic EBT-2 film. AAPM protocol TG-61 (32) was used to measure dose in air and solid water phantoms (Certified Therapy Grade Solid Water: Gammex 457–CTG, Gammex Inc., USA) using a pinpoint PTW chamber (Model N30013) calibrated for 225kV.

The Gafchromic EBT-2 film (Lot# A052810-02AB) used for dosimetry was calibrated by irradiating it with known doses delivered by a Varian 21EX clinical linear accelerator (Varian Associates, Inc.). Two different sets of film, 22 pieces each, were placed in solid water (100 SSD, 1.5 cm depth, with 10 cm backscatter) and irradiated with a range of known doses (0-10 Gy) using a 6 MV beam. An ADCL-calibrated farmer type ion chamber (0.6 cc) was used to verify the dose. With the same batch of film, a calibration curve was also drawn by exposing Gafchromic EBT-2 films

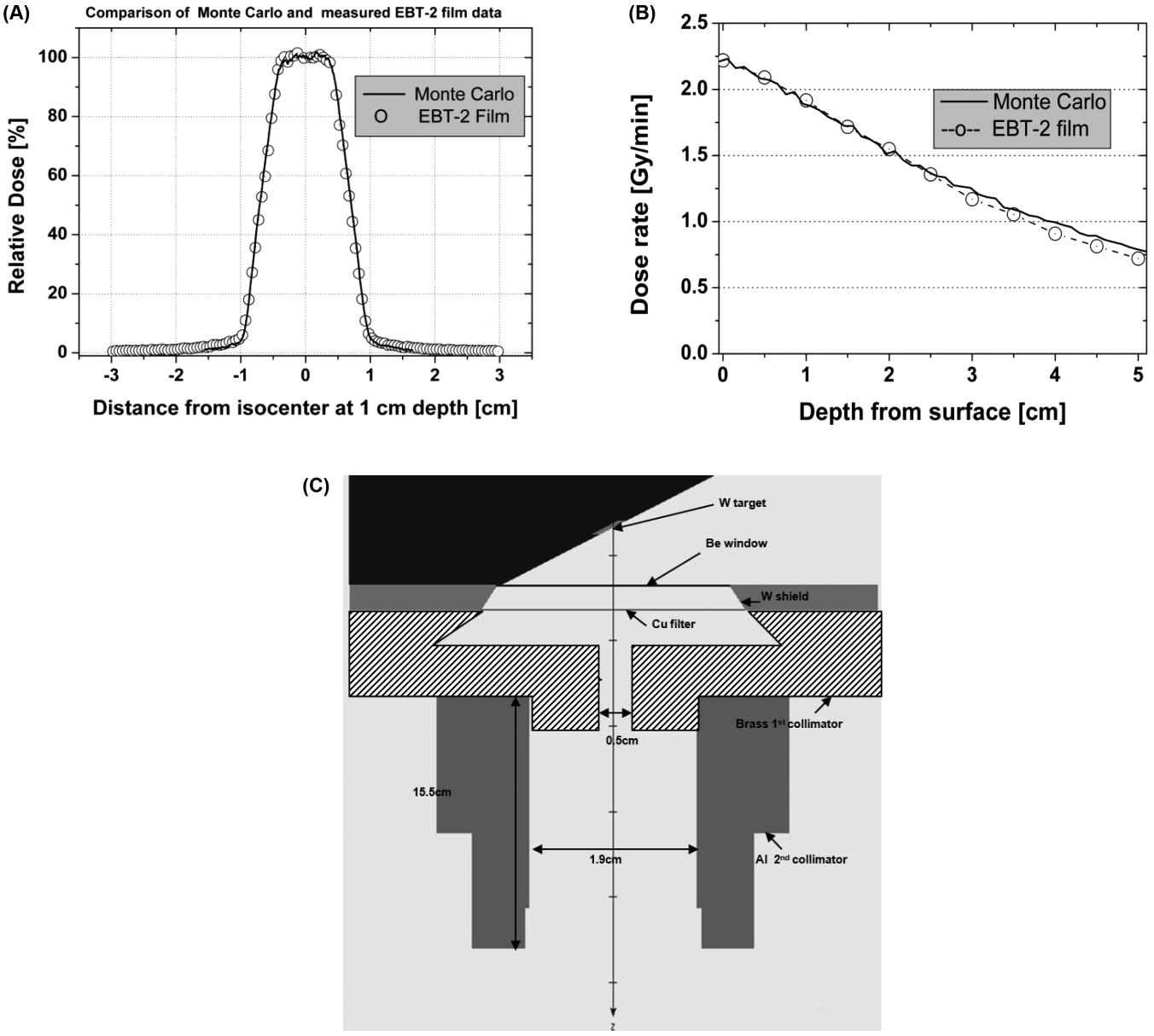

Figure 3: Comparison of Monte Carlo calculations with EBT-2 film dosimetry measurements. (**A**) Comparison of relative dose at 1 cm depth, SSD = 32.5 cm. The solid line represents Monte Carlo calculations and the circles represent film measurements. (**B**) Comparison of depth-dose at 10 mm depth for the heart collimator (SSD = 32.5 cm). The solid line represents Monte Carlo calculations and the circles represent film measurements. (**C**) Schematic of the collimator design rendered by BEAMnrc in X-Z direction.

with the 225 kV X-ray beam at known doses. The measurements showed that the Gafchromic EBT-2 films were energy independent and could effectively be used for measurements of dose in the range of our irradiation experiment (0-10 Gy) using the 225 kV SACRTD (33-35). The dose rate with the secondary collimator at the isocenter was also measured using a pin-point ion chamber (PTW N301013, ADCL calibrated for 225 kV) following the AAPM TG-61 protocol (36). To measure relative depth dose, 11 pieces of Gafchromic EBT-2 film (4 cm × 4 cm) were placed in between 11 slabs of solid water (10 cm × 10 cm × 0.5 cm). The top of the stack of solid water phantom slabs was placed at isocenter (SAD = 32.5) and perpendicular to the beam (225 kV, 13 mA), and the films were exposed to 5 Gy at isocenter. The dose profile distribution at 1 cm depth was also measured with these EBT-2 films. Gafchromic EBT-2 films were analyzed following the process outlined in Devic *et al.* (37). Before irradiation, films were cut into appropriately sized pieces (usually 4 cm × 4 cm) and marked for their orientation. Ten pre-irradiation dark scans (scan without any film) and five pre-irradiation film scans were taken on an Epson V700 flat-bed scanner (Epson Perfection Model: V700 Photo). The dark scans were taken in order to subtract background noise and scanner defects. Post-irradiation scans were done in the same manner, approximately 24 hours after the film irradiations, with the films placed in the positions and orientation as the pre-irradiated film scans. In-house software written in MATLAB was used to acquire the net optical density (OD) distributions to calculate the dose delivered to the film (28).

Animal Holder

A custom-made cylindrical Plexiglas holder (26.6 cm length, 5.71 cm internal diameter, and 3 mm thick, Berg & Son Machine shop, Inc., Little Rock, AR) was designed to hold the rat vertically and allow irradiation of the heart over a full 360 degree rotation (Figure 4). The holder contains two main parts mounted together, the top cylindrical part to hold the rat and the base part to mount it onto the robot palm. In the top 14 cm of the cylindrical part, 2/3 of the Plexiglas was cut away to allow exposure of the heart without interference

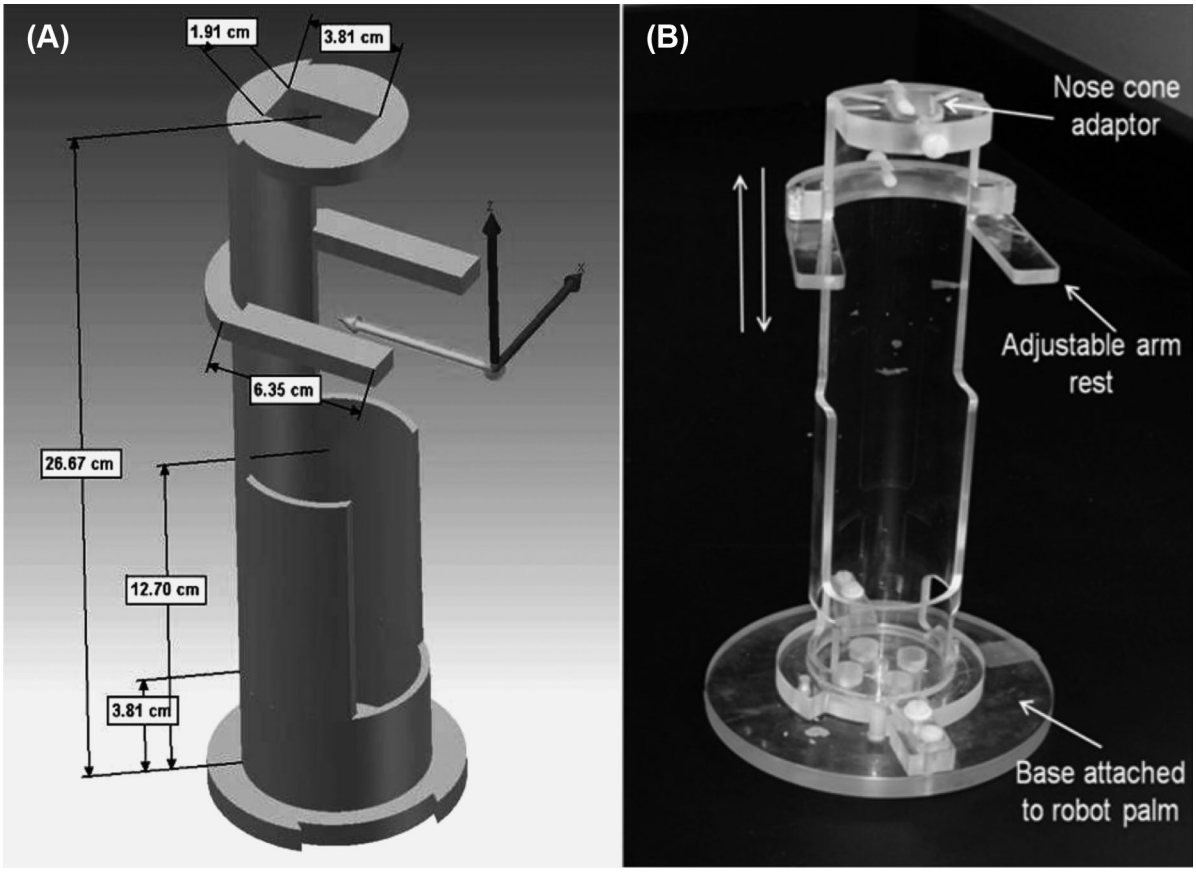

Figure 4: Plexiglas holder for local heart irradiation of the rat. (**A**) Design and dimensions of the holder. (**B**) The holder is mounted on a Plexiglas plate that is attached to the palm of the robotic arm. The rat holder is attached to the base plate by a click and lock mechanism. The nose cone adaptor at the top of the holder has five threaded through holes to hold the nose cone in a fixed position. The front legs of the rat are loosely bound to the adjustable arm-rest. In addition, an elastic band (3 cm wide and 6 cm long) is wrapped around the mid-section of the rat to immobilize the rat in the holder.

of Plexiglas. The remaining 1/3 of the cylinder was used to immobilize the rat. Inhalation anesthesia was used instead of injectable anesthesia, since the latter can reduce tissue oxygenation and affect tissue radiation sensitivity. The nose cone for inhalation anesthesia was held in place by a Plexiglas plate with an oval opening and six threaded thru-holes (M5 screw) mounted on the top of the rat holder. In addition, an adjustable Plexiglas arm-rest (4 cm wide × 1 cm long) was attached to the top segment of the rat holder with an M5 screw that allowed vertical and horizontal positioning (Figure 4). The middle section of the Plexiglas holder was 8.9 cm long and held the mid/lower body of the rat. The bottom section was 3.8 cm long and whenever necessary a small Styrofoam block was placed in this section to adjust the height of the rat being irradiated. The cylindrical animal holder system was attached to a custom-designed circular Plexiglas plate at the base, which was attached to the palm of the robot. The robot was programmed to rotate normal to the X-ray primary beam direction with the rat holder in the vertical position.

Local Heart Irradiation

Before irradiation, the alignment of the primary X-ray beam from the collimator and robot rotation were checked by irradiating a 6 cm × 6 cm piece of Gafchromic EBT-2 film sandwiched in a Styrofoam block at isocenter. The film was irradiated at different angles (0, 90, 180, and 270 degrees) to confirm robotic rotation with the setup alignment with the primary beam central axis. This position was recorded by the robot and the rat heart was aligned to this position for irradiation.

All animal procedures in this study were approved by the Institutional Animal Care and Use Committee of the University of Arkansas for Medical Sciences. The rats used in the study were adult male Sprague-Dawley rats, with ages ranging from 3 to 5 weeks. The rats were anesthetized with 3% isoflurane and placed in the vertical rat holder. The forearms of the rat were held on the arm-rests with soft elastic bands, and an elastic band was placed around the abdomen of the rat to immobilize the rat in the holder. This setup allowed filming in fluoroscopic mode for positioning of the heart at isocenter. For each field, the heart was first visualized using the FPD (using tube setting 70 kV, 5 mA, <1 cGy exposure) and was then placed in the center of the 1.8 cm beam. Figure 5 shows the experimental setup for local heart irradiation and the orthogonal radiographs of a rat recorded before irradiation. Once the heart was localized from the radiographs, the collimator assembly was inserted for the heart irradiation procedure. The assembly consisted of a primary collimator and a secondary collimator with no nozzle inset, giving a beam size of 1.8 cm diameter at 1.0 cm depth, with depth at isocenter. This beam size was found to be sufficient to cover the heart of the 3-5 week old rats. The heart was exposed to 3 fields of 7 Gy each (using 225 kVp, 13 mA), using one AP field and 2 lateral fields. For each field, the robot was used to position the rat and align the target. The FPD was covered with ½ inch of lead during the heart irradiation.

Immunohistochemistry

To confirm radiation targeting of the heart, immunohistochemistry was used to show phosphorylated histone 2Ax (γH2Ax), a marker for DNA damage, and nitrotyrosine, a marker for protein nitrosylation caused by radiation-induced nitrosative stress. For this purpose, hearts and lungs were isolated at 2 hours, 6 hours, 24 hours, and 4 days after irradiation with 21 Gy, or sham-irradiation ($n = 5$). Tissues were fixed in formalin and embedded in paraffin to obtain 5 µm longitudinal sections that were deparaffinized with xylene and then rehydrated. Antigen-retrieval was performed by incubating the sections in 10 mm sodium citrate solution at 90-95°C for 15 minutes. Endogenous peroxidase was blocked with 1% H_2O_2 in methanol for 30 minutes.

For the γH2Ax staining, non-specific antibody binding was reduced with 10% normal donkey serum (Vector Laboratories, Burlingame, CA) in Tris-buffered saline (TBS) containing 3% dry powdered milk and 0.2% bovine serum albumin (BSA). Sections were then incubated with rabbit anti-γH2Ax (Abcam, Cambridge, MA), 1:100 in TBS for 2 hours at room temperature, followed by Alexa Fluor 594-labeled donkey anti-rabbit IgG (Invitrogen, Carlsbad, CA), 1:400 in TBS for 30 minutes. Sections were mounted in SlowFade® antifade reagent containing DAPI counterstain (Invitrogen).

For the nitrotyrosine staining, non-specific antibody binding was reduced with 10% normal goat serum in TBS containing 3% dry powdered milk and 0.2% BSA. Sections were incubated with rabbit anti-nitrotyrosine (Millipore, Billerica, MA), 1:200 in TBS overnight at 4°C. After incubation with biotinylated goat anti-rabbit IgG (Vector Laboratories), 1:400 in TBS for 30 minutes, sections were incubated with pre-formed avidin-biotin-peroxidase complex (Vector Laboratories) for 45 minutes and visualized with 0.5 mg/ml 3,3-diaminobenzidine tetrahydrochloride (Sigma-Aldrich) and 0.003% H_2O_2 in TBS. Sections were counterstained with a light hematoxylin staining.

Histology

Histopathological manifestations of RIHD become apparent long after radiation exposure. To determine long-term changes in our rat model, rats were followed for 6 months after local heart irradiation with a single dose of 21 Gy or sham-irradiation ($n = 9$). At 6 months, hearts and lungs were isolated, fixed in methanol Carnoy's solution

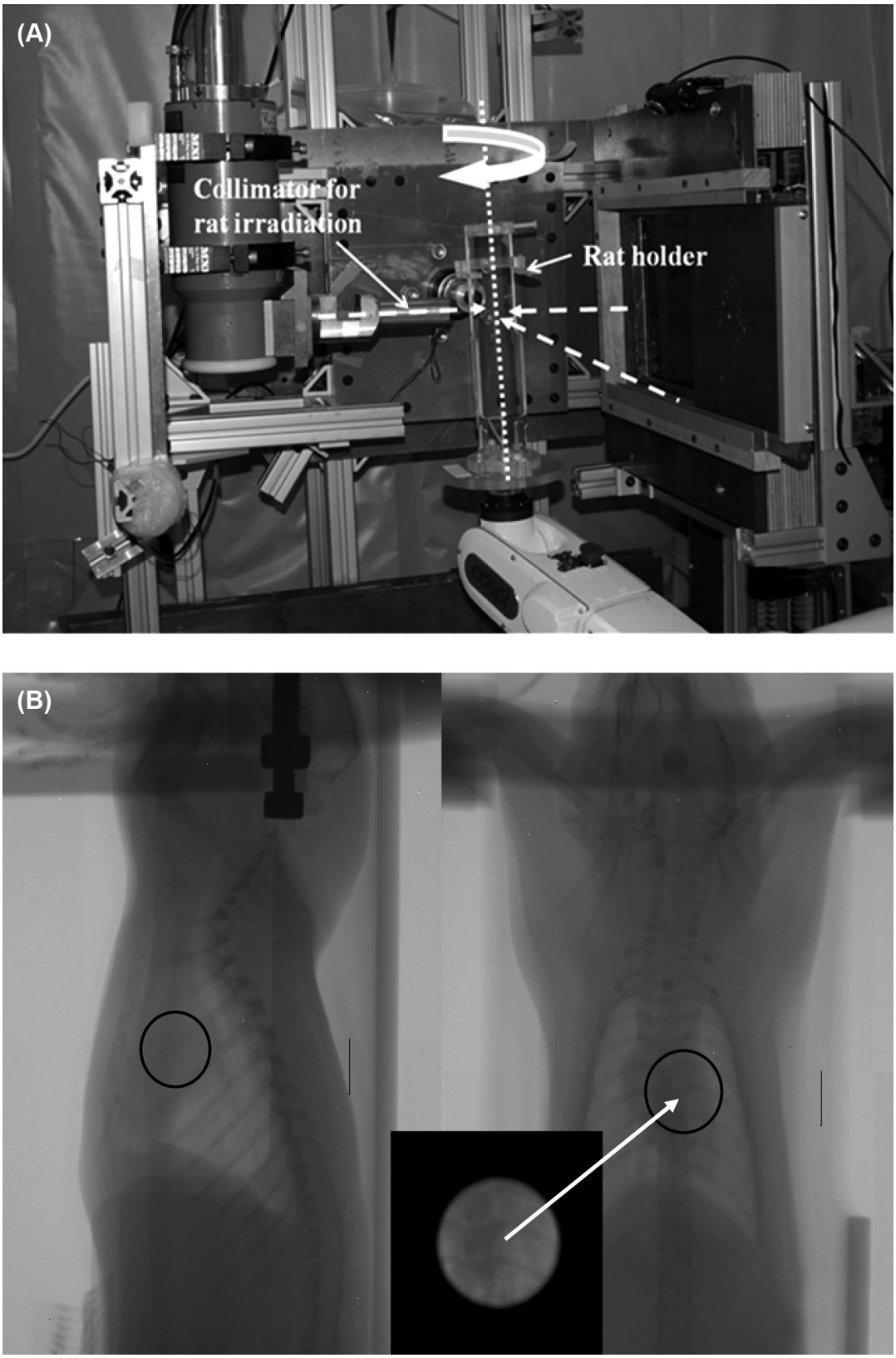

Figure 5: The experimental setup for local rat heart irradiation is shown in (**A**). The rat is held vertically in the holder and is rotated with the robot. The heart is irradiated with three orthogonal beams (dashed arrows): Right Lateral (right to left), Left Lateral (left to right), and Anterior-Posterior. (**B**) Orthogonal radiographs to localize the rat heart. The black circle represents the irradiated target area, and the inset box shows the collimator view of the heart.

(60% methanol, 30% chloroform, 10% acetic acid) and embedded in paraffin. For histopathological analysis, lung sections and longitudinal heart sections of 5 µm were deparaffinized with xylene and rehydrated, followed by a 2 hours incubation in Picrosirius red (American MasterTech, Lodi, CA) supplemented with Fast Green (0.01% w/v, Fisher Scientific, Pittsburgh, PA).

Results and Discussion

Conformal irradiation of the target tissue with minimal exposure of surrounding tissues is one of the key factors in the study of radiobiological mechanisms. This is particularly challenging in pre-clinical studies where the target sizes are often very small. The SACRTD system, as well as other recently developed similar devices (27, 38-42), delivers highly conformal dose distributions with high accuracy and precision to small targets within small laboratory animals, thus narrowing the gap between the current clinical sophistications and the traditional relatively crude radiation techniques used for decades in small animal experimentation.

Film Dosimetry and Monte Carlo Results

Figure 3A shows a dose profile (1cm depth) generated by the SACRTD using the heart collimator. Both Gafchromic EBT-2 film measurements and Monte Carlo calculations are plotted, showing that there was good agreement between the Gafchromic EBT-2 film and Monte Carlo-based results. The Monte Carlo calculation results were normalized to the highest dose point of measured dose rate, applying one factor to all depths. The Monte Carlo simulations, using 4×10^9 simulated photon histories, had a statistical uncertainty of less than 2%. The calculation grid size was 0.5 mm × 0.5 mm × 1.0 mm. Figure 3B shows depth-dose distribution as measured with Gafchromic EBT-2 film plotted against Monte Carlo-based computed depth-dose distribution. Again, the measurements and the calculations were in good agreement.

Our primary collimator was made of a brass cylinder with a narrow opening (0.5 cm in diameter, 5 cm thick). The beam size at isocenter was 15 mm with a penumbra of 1.4 mm (at 80%-20% dose fall-off, Figure 3A), and 18 mm at the target.

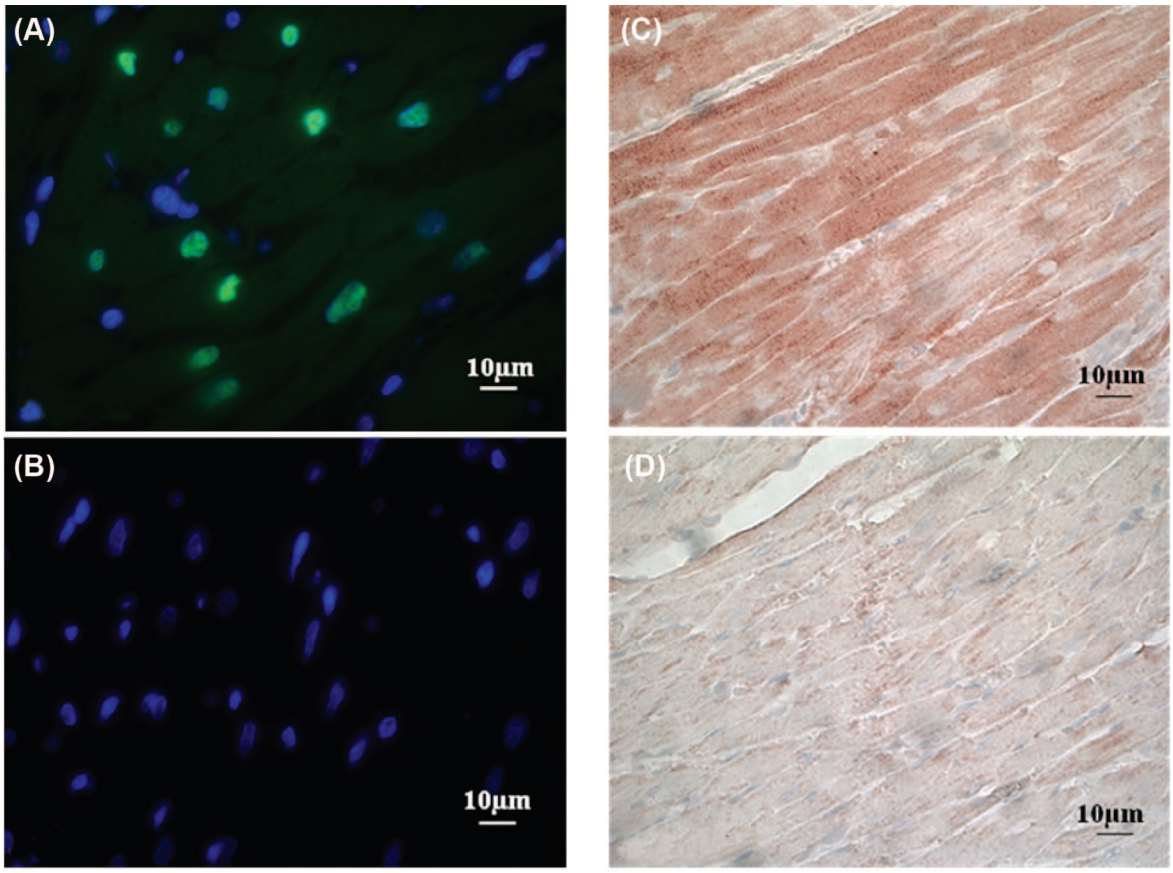

Figure 6: Immunohistochemical verification of cardiac radiation exposure after a total dose of 21 Gy. (**A**) Representative image of the immunofluorescence staining of γH2Ax (green) with DAPI counterstain of nuclei (blue) in the heart at 2 hours after irradiation. (**B**) Representative image of the immunofluorescence staining of γH2Ax with DAPI counterstain of nuclei in the heart at 2 hours after control treatment (sham-irradiation). No γH2Ax was detected after sham-irradiation. (**C**) Representative image of the immunohistochemical staining of nitrotyrosine in the heart at 6 hours after irradiation. (**D**) Representative image of the immunohistochemical staining of nitrotyrosine in the heart at 6 hours after sham-irradiation. Minimal nitrotyrosine was detected after sham-irradiation.

This beam size was sufficient to cover the heart of the 3-4 week old rats used in our model. In order to be more flexible in irradiating rats with different heart sizes, the robotic setup allows to change SAD, which ultimately changes beam diameter at the robot rotation axis. With Monte Carlo calculations and film measurements we can estimate doses at the new position. In addition, we aim to minimize the penumbra as much as possible with a newly designed brass shielding attachment collimator. Monte Carlo based calculation tools will first be used to design and characterize the beam at different depth.

Method of Local Heart Irradiation

Our previous method for *in vivo* rat heart irradiation involved parallel opposed fields (AP, PA 1:1). For this purpose, rats were placed in a Plexiglas jig with lead shielding plates. A circular hole in the lead plates provided a 19 mm field for exposure of the heart (19). The previous method assumed the same anatomy for rats of the same size. The new method described in this article has several advantages. In an attempt to reduce radiation dose to surrounding normal tissues, especially the spinal cord, the heart was irradiated using three beams at 90° angles from each other, whereby the spine was in the path of one of the three X-ray beams only. By reducing the dose to the spinal cord, the chance of paralysis was reduced at later time points after irradiation, thus minimizing potential confounding effects. The three-beam technique was facilitated by radiographic localization with the use of the built-in X-ray imager and accurate and precise positioning of the rat with the use of the robotic arm. Imaging was performed with low X-ray energy, and the radiation imaging doses were <1 cGy. Although not shown here, targets of different sizes can be accommodated with different collimators giving different field sizes. This method will also be appropriate for studies in which only certain anatomical parts of the heart need to be irradiated. The total amount of time for animal preparation, setup and irradiation with the current method is close to the total time that was required for our previous AP-PA local heart irradiation method.

Immunohistochemical Confirmation of Heart Exposure

Long-term myocardial injury and cardiac functional changes have been observed in rats exposed to 15-25 Gy to the heart (13-18, 43). We therefore chose a single dose of 21 Gy for biological verification of cardiac exposure in our rat model of heart irradiation. Hearts and lungs were isolated at time points from 2 hours to 4 days after irradiation to perform immunohistochemical analysis of γH2Ax, a marker for DNA damage caused by radiation-induced oxidative stress, and nitrotyrosine, a marker for protein nitrosylation caused by nitrosative stress. Figure 6 shows

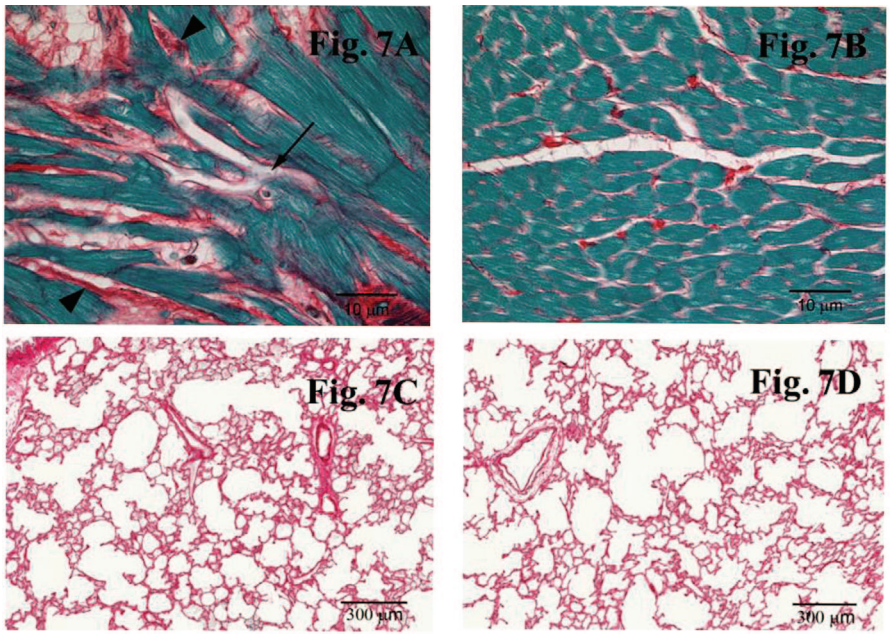

Figure 7: Representative images of the histopathological analysis with Picrosirius red and Fast Green at 6 months after local heart irradiation with a total dose of 21 Gy. Extracellular matrix stains red, while cytoplasm stains green. (**A**) Representative image of the histological staining of the heart at 6 months after 21 Gy. Local irradiation caused myocardial degeneration (arrow) and fibrosis (arrowheads) in the heart. (**B**) Representative image of the histological staining of the heart at 6 months after control treatment (sham-irradiation). Minimal myocardial degeneration and fibrosis was detected in the heart of control animals. (**C**) Representative image of the histological staining of the lung at 6 months after local heart irradiation with 21 Gy. No histopathological evidence of damage was detected in the lung. (**D**) Representative image of the histological staining of the lung at 6 months after sham-irradiation.

representative immunofluorescence stainings of γH_2Ax with DAPI counterstain of nuclei. The γH2Ax foci were observed only in irradiated hearts, indicating the presence of radiation-induced DNA double strand breaks. The γH2Ax foci were most prominent at 2 hours after irradiation, which is in agreement with the known DNA repair that occurs immediately after exposure to ionizing radiation. As expected, only a few γH2Ax foci were observed in the lungs (data not shown), confirming that exposure of the lungs was significantly less than exposure of the heart. Figure 6C and D show immunohistochemical stainings of nitrotyrosine. Nitrotyrosine staining was observed evenly distributed in irradiated hearts, indicating nitrosative stress as a result of uniform radiation exposure. Minimal nitrotyrosine staining was observed in the lung samples, indicating that exposure of the lungs were below the detection limit of our immunohistochemical analysis.

Histopathological Analysis of Cardiac Radiation Injury

Rats were followed for 6 months after local heart irradiation with a single dose of 21 Gy. At 6 months, all irradiated hearts showed myocardial degeneration and fibrosis, which are typical long-term histopathological manifestations of cardiac radiation injury (Figure 7). Although about 10% of the lungs showed macroscopic evidence of radiation exposure (small white spots on the lung surface), no histopathological evidence of damage was found (data not shown). These results show that our method of image-guided local heart irradiation in the rat is an appropriate pre-clinical model of RIHD. In conclusion, we here present a method of local heart irradiation in rats that uses a small animal conformal radiation platform developed at our institution to allow image-guided irradiation of the heart from multiple angles.

Acknowledgements

This work was supported in part by the American Cancer Society (Research Scholar Grant 10-125-01-CCE) and the National Institutes of Health (R01 CA148679). The work is also supported by UAMS MRE grant (G1–37238–01) and Arkansas Biomedical Institute (ABI, UAMS Tobacco Settlement Fund).

Conflicts of Interest

None.

References

1. Adams MJ, Hardenbergh PH, Constine LS & Lipshultz SE. Radiation-associated cardiovascular disease. *Critical Reviews in Oncology/Hematology 45*, 55-75 (2003). DOI: 10.1016/j.bbr.2011.03.031
2. Senkus-Konefka EB & Jassem J. Cardiovascular effects of breast cancer radiotherapy. *Cancer Treatment Reviews 33*, 578-593 (2007). DOI: 10.1016/j.ctrv.2007.07.011
3. Taylor CW, McGale P & Darby SC. Cardiac Risks of Breast-cancer Radiotherapy: A Contemporary View. *Clinical Oncology 18*, 236-246 (2006). DOI: 10.1016/j.clon.2005.11.003
4. Heidenreich PA, Hancock SL, Vagelos RH, Lee BK & Schnittger, I. Diastolic dysfunction after mediastinal irradiation. *American Heart Journal 150*, 977-982 (2005). DOI: 10.1016/j.ahj.2004.12.026
5. Chera BS, Rodriguez C, Morris CG, Louis D, Yeung D, Li Z & Mendenhall NP. Dosimetric comparison of three different involved nodal irradiation techniques for Stage II Hodgkin's Lymphoma patients: conventional radiotherapy, intensity-modulated radiotherapy, and three-dimensional proton radiotherapy. *International Journal of Radiation Oncology*Biology*Physics 75*, 1173-1180 (2009). DOI: 10.1016/j.ijrobp.2008.12.048
6. Hong TS, Crowley EM, Killoran J & Mamon HJ. Considerations in treatment planning for esophageal cancer. *Semin Radiat Oncol 17*, 53-61 (2007). DOI: 10.1016/j.semradonc.2006.09.001
7. McGale P & Darby SC. Low doses of ionizing radiation and circulatory diseases: a systematic review of the published epidemiological evidence. *Radiat Res 163*, 247-257 (2005). DOI: 10.1667/RR3314
8. Tillman GF, Pawlicki T, Koong AC & Goodman KA. Preoperative versus postoperative radiotherapy for locally advanced gastroesophageal junction and proximal gastric cancers: a comparison of normal tissue radiation doses. *Dis Esophagus 21*, 437-444 (2008). DOI: 10.1111/j.1442-2050.2007.00794.x
9. Weber DC, Peguret N, Dipasquale G & Cozzi L. Involved-node and involved-field volumetric modulated arc vs. fixed beam intensity-modulated radiotherapy for female patients with early-stage supradiaphragmatic hodgkin lymphoma: a comparative planning study. *Int J Radiat Oncol Biol Phys 75*, 1578-1586 (2009). DOI: 10.1016/j.ijrobp.2009.05.012
10. Wu WC, Chan CL, Wong YW & Cuijpers JP. A study on the influence of breathing phases in intensity-modulated radiotherapy of lung tumours using four-dimensional CT. *Br J Radiol 83*, 252-256 (2009). DOI: 10.1259/bjr/33094251
11. Zhang X, Li Y, Pan X, Xiaoqiang L, Mohan R, Komaki R, Cox JD & Chang JY. Intensity-modulated proton therapy reduces the dose to normal tissue compared with intensity-modulated radiation therapy or passive scattering proton therapy and enables individualized radical radiotherapy for extensive Stage IIIB non-small-cell lung cancer: a virtual clinical study. *Int J Radiat Oncol Biol Phys 77*, 357-366. DOI: 10.1016/j.ijrobp.2009.04.028
12. Taylor CW, Povall JM, McGale P, Nisbet A, Dodwell D, Smith JT & Darby SC. Cardiac dose from tangential breast cancer radiotherapy in the year 2006. *Int J Radiat Oncol Biol Phys 72*, 501-507 (2008). DOI: 10.1016/j.ijrobp.2007.12.058
13. Kitahara T, Liu K, Solanki K & Trott KR. Functional and morphological damage after local heart irradiation and/or adriamycin in Wistar rats. *Radiation Oncology Investigations 1*, 198-205 (1993). DOI: 10.1002/roi.2970010403
14. Kruse JJ, Zurcher C, Strootman EG, Bart CI, Schlagwein N, Leer JW & Wondergem J. Structural changes in the auricles of the rat heart after local ionizing irradiation. *Radiother Oncol 58*, 303-311 (2001). DOI: 10.1016/S0167-8140(00)00327-3
15. Lauk S, Kiszel Z, Buschmann J & Trott KR. Radiation-induced heart disease in rats. *International Journal of Radiation Oncology, Biology, Physics 11*, 801-808 (1985). DOI: 10.1016/0360-3016-(85)90314-1
16. Franken NA, Camps JA, Van Ravels FJ, van der Laarse A, Pauwels EK & Wondergem J. Comparison of in vivo cardiac function with ex vivo cardiac performance of the rat heart after thoracic irradiation. *Br J Radiol 70*, 1004-1009 (1997). DOI: bjr.birjournals.org/content/70/838/1004.full.pdf+html

17. Boerma M, Wang J, Wondergem J, Joseph J, Qiu X, Kennedy RH & Hauer-Jensen M. Influence of mast cells on structural and functional manifestations of radiation-induced heart disease. *Cancer Res 65*, 3100-3107 (2005). DOI: 10.1016/j.ijrobp.2008.04.042
18. Wondergem J, van der Laarse A, Van Ravels FJ, van Wermeskerken AM, Verhoeve HR, de Graaf BW & Leer JW. In vitro assessment of cardiac performance after irradiation using an isolated working rat heart preparation. *Int J Radiat Biol 59*, 1053-1068 (1991). DOI: 10.1080/09553009114550931
19. Boerma M, Roberto KA & Hauer-Jensen M. Prevention and treatment of functional and structural radiation injury in the rat heart by pentoxifylline and alpha-tocopherol. *Int J Radiat Oncol Biol Phys 72*, 170-177 (2008). DOI: 10.1016/j.ijrobp.2008.04.042
20. Verhaegen F, Granton P & Tryggestad E. Small animal radiotherapy research platforms. *Phys Med Biol 56*, R55-83 (2011). DOI: 10.1088/0031-9155/56/12/r01
21. Sharma S. SU-E-T-312: development of a rat model of radiation induced heart disease using SACRTD. *Med Phys 38*, 3559 (2011). DOI: 10.1118/1.3612263
22. Sharma S, Chao M, Moros E & Corry P. TH-C-BRC-08: Integration of cone beam CT imaging and a small animal conformal RT device using a 6DOF robotic arm. *Med Phys 36*, 2799 (2009). DOI: 10.1118/1.3182622
23. Sharma S, Chao M, Yan Y, Corry P & Moros E. SU-E-I-15: CBCT using a robotic-arm based small animal irradiation system. *Med Phys 38*, 3398-3399 (2011). DOI: 10.1118/1.3611588
24. Sharma S, Moros E & Corry P. SU-GG-J-160: Radiation enclosure shielding calculations for a laboratory-based small animal conformal radiation therapy device. *Med Phys 35*, 2716 (2008). DOI: 10.1118/1.2961709
25. Sharma S, Moros E & Corry P. SU-GG-J-170: Small animal conformal radiation therapy device. *Med Phys 35*, 2718 (2008). DOI: 10.1118/1.2961719
26. Sharma S, Webber J, Nathan K, Griffin R, Moros E & Corry P. SU-FF-J-160: Spatially fractionated radiation therapy (GRID) on implanted tumors using a small animal conformal radiation therapy system. *Med Phys 36*, 2514 (2009). DOI: 10.1118/1.3181453
27. Wong J, Armour E, Kazanzides P, Iordachita I, Tryggestad E, Deng H, Matinfar M, Kennedy C, Liu Z, Chan T, Gray O, Verhaegen F, McNutt T, Ford E & DeWeese TL. High-resolution, small animal radiation research platform with X-ray tomographic guidance capabilities. *International Journal of Radiation Oncology*Biology*Physics 71*, 1591-1599 (2008). DOI: 10.1016/j.ijrobp.2008.04.025
28. Clarkson R, Lindsay PE, Ansell S, Wilson G, Jelveh S, Hill RP & Jaffray DA. Characterization of image quality and image-guidance performance of a preclinical microirradiator. *Medical Physics 38*, 845-856 (2011). DOI: 10.1118/1.3533947
29. Adept Viper S650/S850 Manual, A. T. I. Livermore, CA 94551.
30. XRD 0820AN Reference Manual, Perkin Elmer Inc., Santa Clara, CA 95054.
31. Magdalena B, Hu Z, Paul JK & Edward EG. Kilovoltage beam Monte Carlo dose calculations in submillimeter voxels for small animal radiotherapy. *Med Phys 36*, 4991-4999 (2009). DOI: 10.1118/1.3238465
32. Yoo S. Clinical implementation of AAPM TG61 protocol for kilovoltage x-ray beam dosimetry. *Med Phys 29*, 2269 (2002). DOI: 10.1118/1.1508376
33. Chiu-Tsao S. Energy dependence of response of new high sensitivity radiochromic films for megavoltage and kilovoltage radiation energies. *Med Phys 32*, 3350 (2005). DOI: 10.1118/1.2955746
34. Zeil K, Beyreuther E, Lessmann E, Wagner W & Pawelke J. Cell irradiation setup and dosimetry for radiobiological studies at ELBE. *Nuclear Instruments and Methods in Physics Research Section B: Beam Interactions with Materials and Atoms 267*, 2403-2410 (2009). DOI: 10.1016/j.nimb.2009.04.015
35. Lindsay P, Rink A, Ruschin M & Jaffray D. Investigation of energy dependence of EBT and EBT-2 Gafchromic film. *Med Phys 37*, 571. DOI: 10.1118/1.3291622
36. Chair CMM, Coffey CW, DeWerd LA, Liu C, Nath R, Seltzer SM & Seuntjens JP. AAPM protocol for 40–300 kV x-ray beam dosimetry in radiotherapy and radiobiology. *Medical Physics 28*, 868-893 (2001). DOI: 10.1118/1.1374247
37. Devic S. Precise radiochromic film dosimetry using a flat-bed document scanner. *Med Phys 32*, 2245 (2005). DOI: 10.1118/1.1929253
38. Sigen Wang ZL, Sultana S, Schreiber E, Zhou O, Chang S. A novel high resolution micro-radiotherapy system for small animal irradiation for cancer research. *BioFactors 30*, 265-270 (2007). DOI: 10.1002/biof.5520300408
39. Stojadinovic S, Low DA, Hope AJ, Vicic M, Deasy JO, Cui J, Khullar D, Parikh PJ, Malinowski KT, Izaguirre EW, Mutic S & Grigsby PW. MicroRT–Small animal conformal irradiator. *Medical Physics 34*, 4706-4716 (2007). DOI: 10.1118/1.2799887
40. Strahinja S, Daniel AL, Milos V, Sasa M, Joseph OD, Andrew JH, Parag JP & Perry WG. Progress toward a microradiation therapy small animal conformal irradiator. *Medical Physics 33*, 3834-3845 (2006). DOI: 10.1118/1.2349693
41. Weng X, Yan Y & Ratanatharathorn V. SU-GG-J-36: Application of Gafchromic XR-RV2 film for small animal irradiation dosimetry. *Med Phys 35*, 2687-2687 (2008). DOI: 10.1118/1.2961594
42. Woo MK, *et al*. Commissioning and evaluation of a new commercial small rodent x-ray irradiator. *Biomed Imaging Interv J 2(1)*, *e10* (2006). DOI: 10.2349/biij.2.1.e10
43. Hu S, Chen Y, Li L, Chen J, Wu B, Zhou X, Zhi G, Li Q, Wang R, Duan H, Guo Z, Yang Y, Xiao F, Wang H & Wang L. Effects of adenovirus-mediated delivery of the human hepatocyte growth factor gene in experimental radiation-induced heart disease. *Int J Radiat Oncol Biol Phys 75*, 1537-1544 (2009). DOI: 10.1016/j.ijrobp.2009.07.1697

Received: December 5, 2012; Revised: January 28, 2013; Accepted: January 30, 2013